Dielectric Spectroscopy Using Monopole Antennas of General Electrical Length

WAYMOND R. SCOTT, JR., MEMBER, IEEE, AND GLENN S. SMITH, FELLOW, IEEE

Abstract—**A procedure is developed for measuring the complex dielectric permittivity of a material over a broad range of frequencies using a monopole antenna. No restrictions are placed on the electrical size of the antenna. The antenna is calibrated one time by measuring the input admittance in a standard medium with known permittivity, such as air. Next, the admittance is measured with the antenna immersed in a material with unknown permittivity. These two sets of admittances are then used to determine the permittivity of the material. As an application of the procedure, the complex permittivity of the alcohol 1-butanol and saline solutions were measured using a cylindrical monopole antenna. The measured permittivities are in good agreement with those determined by previous investigators.**

I. Introduction

THE DETERMINATION of the complex dielectric permittivity of a material from the measured input impedance (admittance) of a monopole antenna immersed in the material is discussed. In particular, the complex permittivity is to be determined with a single antenna over a broad range of frequencies, a typical range being f to 200 f. Thus, the electrical size of the antenna in the material can range from electrically small to electrically large.

The use of antennas for dielectric measurements has been discussed in the past, and a brief review of the subject is presented in a recent paper [1]. A systematic procedure for the measurement was also introduced in that paper. This procedure has the following steps.

1) The input impedance of the antenna is measured over a range of frequencies with the antenna in a standard medium with a *known* permittivity, such as air. This can be viewed as a calibration of the antenna.
2) The impedance obtained in step 1) is used in the construction of a function which determines the input impedance of the antenna when it is immersed in a medium of general permittivity.
3) The antenna is inserted into the medium whose permittivity is to be determined, and the impedance of the antenna is measured over a range of frequencies. The measured impedance is then used with the inverse of the function obtained in step 2) to determine the complex permittivity of the material.

Manuscript received November 19, 1985; revised February 7, 1986. This work was supported in part by the Joint Services Electronics Program under Contracts DAAG29-81-K-0024 and DAAG29-84-K-0024.

The authors are with the School of Electrical Engineering, Georgia Institute of Technology, Atlanta, GA 30332.

IEEE Log Number 8609026.

In the previous paper [1], a rational function was used in step 2) to express the impedance in terms of the permittivity. For a rational function of order three, the measurement procedure was shown to be accurate when the antenna was less than or equal to resonant size, e.g., $|kh| \lesssim 1.5$ for a cylindrical monopole of height h in a medium with wavenumber k. The extension of the procedure to higher order rational functions and, therefore, to electrically larger antennas appears to be difficult.

It would clearly be advantageous to modify the measurement procedure outlined above so that it is viable for antennas with unrestricted electrical size. This is accomplished in this paper by using a numerical procedure to form the functional relationship between the input impedance of the antenna and the complex permittivity of the surrounding medium (step 2). To demonstrate the accuracy of the procedure, the complex permittivities of standard liquids were measured using cylindrical monopole antennas of electrical size as large as $|kh| = 19$. The measured permittivities for these liquids are in good agreement with those obtained by previous investigators.

II. Formulation of the Measurement Procedure

Fig. 1(a) is a diagram of a monopole antenna driven from a coaxial transmission line. The material with complex effective permittivity $\tilde{\epsilon}_r = \tilde{\epsilon}_r' - j\tilde{\epsilon}_r''$ surrounds the monopole antenna and extends into the coaxial line to the depth h_i. The permeability of the material is assumed to be $\mu = \mu_0$. The dimensions of the coaxial line are chosen so that the transverse electromagnetic (TEM) mode is the only propagating mode in the line when it is filled with the material. When the material extends into the line to a depth greater than approximately $(b - a)$, the field in the coaxial line is approximately TEM at the interface ($A - A'$ in Fig. 1) between the material and the insulation, and a TEM input admittance for the antenna can be defined at this interface. The input admittances for the antenna in two different materials, 1 and 2, are simply related [1], [2]:

$$\frac{Y(s_1, \tilde{\epsilon}_{r1})}{\sqrt{\tilde{\epsilon}_{r1}}} = \frac{Y(s_2, \tilde{\epsilon}_{r2})}{\sqrt{\tilde{\epsilon}_{r2}}} \tag{1a}$$

provided

$$s_1\sqrt{\tilde{\epsilon}_{r1}} = s_2\sqrt{\tilde{\epsilon}_{r2}}\,. \tag{1b}$$

Here, $s = \sigma + j\omega$ is the complex frequency.

Using these equations, a normalized input admittance $W(s, \tilde{\epsilon}_r)$ is defined for the antenna; this can be expressed as a

0018-926X/86/0700-0919$01.00

function $f(S)$ of the single complex parameter S:[1]

$$W(s,\ \tilde{\epsilon}_r) \equiv \frac{sh}{cY_0}\, Y(s,\ \tilde{\epsilon}_r) = f(S) \tag{2a}$$

with the normalized propagation constant

$$S \equiv \frac{h\sqrt{\tilde{\epsilon}_r}}{c}\, s, \tag{2b}$$

where c is the speed of light in free space. The monopole can have any physical shape, and h can be any physical dimension of the antenna. The cylindrical monopole of height h is used for convenience in the discussion. Y_0 is the characteristic admittance of the coaxial line feeding the monopole.

The purpose of this analysis is to determine the complex permittivity $\tilde{\epsilon}_r$ over a broad range of frequencies from the measured input admittance of the antenna. This is accomplished with a three-step procedure.

1) The first step is to make a one-time calibration of the antenna. The input admittance $Y(j\omega,\ \tilde{\epsilon}_{rs})$ is measured over a broad range of real frequencies with the antenna immersed in a standard medium of known complex permittivity $\tilde{\epsilon}_{rs}$. The normalized admittance $W(j\omega,\ \tilde{\epsilon}_{rs})$ is then formed. This determines $f(S)$ along a line in the complex S-plane. For the remainder of the discussion, the standard medium is assumed to be air, so that $\tilde{\epsilon}_{rs} = 1$ and $S = j\omega h/c$. The line in the S plane for the calibration is then along the imaginary axis.
2) Values of $f(S)$ at general S are obtained by analytically continuing the data from the line. A method for performing the analytic continuation is presented later.
3) The input admittance $Y(j\omega,\ \tilde{\epsilon}_r)$ is measured over a broad range of frequencies with the antenna immersed in the material of unknown complex permittivity $\tilde{\epsilon}_r$. The normalized input admittance $W(j\omega,\ \tilde{\epsilon}_r)$ is used with the inverse of $f(S)$ to obtain S:

$$S = f^{-1}[W(j\omega,\ \tilde{\epsilon}_r)], \tag{3}$$

and finally the complex permittivity is obtained from S:

$$\tilde{\epsilon}_r = -\left(\frac{Sc}{\omega h}\right)^2. \tag{4}$$

The open-circuited coaxial line shown in Fig. 1(b) is a structure whose electrical performance is similar to that of the cylindrical monopole antenna shown in Fig. 1(a). The monopole can very crudely be thought of as the coaxial line with the outer conductor folded down to form the image plane. The normalized input admittance for the coaxial line, unlike that for the antenna, has a simple analytical representation:

$$W(j\omega,\ \tilde{\epsilon}_r) = f(S) = S\ \tanh\ (S). \tag{5}$$

Here, S is given by (2b) with h replaced by the effective length l of the transmission line. The open-circuited coaxial line has been studied in detail in [3] as a sample cell for dielectric spectroscopy, and the knowledge gained from that study will be used to assist in the discussion of the monopole antenna.

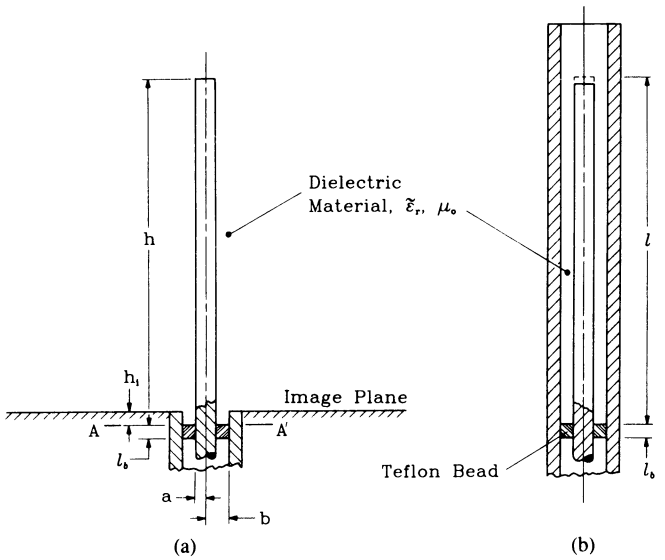

Fig. 1. (a) Monopole antenna fed from a coaxial line. (b) Open-circuited coaxial line.

III. Analytic Continuation

The antenna is calibrated by measuring the reflection coefficient $\rho(j\omega,\ \tilde{\epsilon}_{rs})$ at its terminals, over the frequency range $0 \leqslant \omega \leqslant \omega_{\max}$, when it is immersed in the standard medium—air with $\tilde{\epsilon}_{rs} = 1$. The input admittance is then determined from

$$Y = Y_0 \left(\frac{1-\rho}{1+\rho}\right), \tag{6}$$

and the normalized admittance W is obtained from (2a). This determines the function $f(S)$ along a segment of the imaginary axis in the S plane

$$0 \leqslant S \leqslant j\omega_{\max} h/c. \tag{7}$$

The function $f(S)$ is analytically continued from this line into the right half of the S plane by first analytically continuing the reflection coefficient ρ in the s plane, and then obtaining $f(S)$ using (6) and (2). The reflection coefficient is analytically continued because it is generally well behaved along the imaginary axis in the s plane, $|\rho| \leqslant 1.0$. In contrast, the admittance can have singularities close to or along the imaginary axis. For example, the admittance for the open-circuited coaxial line, Fig. 1(b), has poles on the imaginary axis at $S = j(2n+1)\pi/2$, $n = 0, 1, 2, \cdots$. Note that both the reflection coefficient and the admittance have no singularities in the right half of the s plane or S plane.

Now consider the analytic continuation of the reflection coefficient in the $s = \sigma + j\omega$ plane. From the definition of the two-sided Laplace transform

$$\rho(s) = \int_{-\infty}^{\infty} h(t)e^{-st}\, dt, \tag{8}$$

[1] Note that the normalized admittance is different from the normalized admittance defined in [1].

where $h(t)$ represents the reflection of an impulse from the terminals of the antenna. Since $h(t)$ is causal, viz, $h(t) = 0$ for $t < 0$, (8) can be changed to

$$\rho(s) = \int_{-\infty}^{\infty} h(t) e^{-\sigma|t|} e^{-j\omega t}\, dt. \tag{9}$$

This is the Laplace transform with $s = j\omega$ of the product of $h(t)$ and exp $(-\sigma|t|)$. Thus, $\rho(s)$ can be expressed as the convolution of two frequency-domain quantities:

$$\rho(s) = \frac{1}{2\pi} \rho(j\omega) * G(j\omega;\ \sigma)$$

$$= \frac{1}{2\pi} \int_{-\infty}^{\infty} \rho(j\omega - j\lambda) G(j\lambda;\ \sigma)\, d\lambda, \tag{10}$$

where

$$G(j\omega;\ \sigma) = \frac{2\sigma}{\sigma^2 + \omega^2}. \tag{11}$$

Note that $\sigma > 0$ for the existence of the Laplace transform of exp $(-\sigma|t|)$. Thus, (10) can be used to analytically continue ρ from the imaginary axis, $s = j\omega$, into the right half of the s plane, but it cannot continue ρ into the left half of the s plane.

Equation (10) assumes that the reflection coefficient is known for all frequencies ω, but recall that the reflection coefficient is only measured for $0 \leqslant \omega \leqslant \omega_{max}$. Let $\rho(j\omega)$ be expressed as

$$\rho(j\omega) = \rho_<(j\omega) + \rho_>(j\omega), \tag{12}$$

where

$$\begin{aligned} \rho_<(j\omega) &= \rho(j\omega) && |\omega| \leqslant \omega_{max} \\ &= 0 && |\omega| > \omega_{max} \\ \rho_>(j\omega) &= 0 && |\omega| \leqslant \omega_{max} \\ &= \rho(j\omega) && |\omega| > \omega_{max}. \end{aligned} \tag{13}$$

In addition, let $N(s)$ be a causal window function that has a magnitude approximately equal to one when $s = j\omega$, $|\omega| \leqslant \omega_{max}$ and approximately equal to zero when $s = j\omega$, $|\omega| > \omega_{max}$. When (10) is used to analytically continue the product $\rho(j\omega)N(j\omega)$, the following result is obtained:

$$\rho(s)N(s) = \frac{1}{2\pi} [\rho_<(j\omega)N(j\omega) + \rho_>(j\omega)N(j\omega)] * G(j\omega;\ \sigma)$$

or

$$\rho(\sigma + j\omega) = \frac{[\rho_<(j\omega)N(j\omega)] * G(j\omega;\ \sigma)}{2\pi N(\sigma + j\omega)} + \frac{[\rho_>(j\omega)N(j\omega)] * G(j\omega;\ \sigma)}{2\pi N(\sigma + j\omega)}. \tag{14}$$

The first term on the right of (14) can be evaluated since $\rho_<(j\omega)$ is measured; the second term, however, cannot be evaluated since $\rho_>(j\omega)$ is not known. Thus, the second term represents the error that results from continuing the reflection coefficient from values along the segment of the imaginary axis $|\omega| \leqslant \omega_{max}$ rather than from values along the entire imaginary axis. This error can be made small by proper choice of the window function $N(s)$.

Graphical representations for the various functions in (14) are shown in Fig. 2. From the graphs, it is clear that the relative error in the continuation, which is proportional to $|(\rho_> N) * G| / |(\rho_< N) * G|$, can be made very small for $s = \sigma + j\omega$, $|\omega| \lesssim \omega_{max}$ by using a window function with a sharp cutoff near $|\omega| = \omega_{max}$. Thus, the analytic continuation of the reflection coefficient from the imaginary axis is well approximated by

$$\rho(\sigma + j\omega) = \frac{[\rho_<(j\omega)N(j\omega)] * G(j\omega;\ \sigma)}{2\pi N(\sigma + j\omega)} \tag{15}$$

for $|\omega| \lesssim \omega_{max}$.

In this work, an elliptic filter is used as a causal window function $N(s)$. The reflection coefficient $\rho(j\omega)$ is measured at discrete points on the range $0 \leqslant \omega \leqslant \omega_{max}$, and a complex cubic spline is fit to these data. An efficient procedure, based on the window function being a rational function, was developed for performing the convolution integral in (15); this is described in [4].

A numerical simulation was performed to demonstrate the accuracy of the analytic continuation procedure. The normalized admittance of the open-circuited coaxial line (5) was used to obtain the reflection coefficient for this example. The reflection coefficient was computed at 181 discrete points along the $j\omega$ axis for $0 \leqslant \omega \leqslant \omega_{max}$, with $\omega_{max} l/c = 19.6$. This corresponds to a line of effective length $l = 5.2$ cm and a maximum frequency $f_{max} = 18.0$ GHz. The elliptic filter used as the causal window function had a passband ripple of 1 dB, a cutoff frequency of $0.99\ \omega_{max}$, and a stop-band attenuation of 40 db.

The reflection coefficient was analytically continued from the imaginary axis into the right half of the s plane using (15). The function $f(S)$ was then computed, and the error in $f(S)$ that is a result of the continuation was evaluated. The error is defined as

$$E_c(S) \equiv \left| \frac{f_c(S) - f(S)}{f(S)} \right|. \tag{16}$$

Here, $f_c(S)$ is obtained from the analytic continuation of $\rho(s)$, and $f(S)$ is obtained from the analytic expression for the reflection coefficient ((5) with (6) and (2)). Fig. 3(a) is a contour graph of this error in the normalized S plane, $S_n = S/(\omega_{max} l/c)$. Note that the procedure can analytically continue the function $f(S)$ from the imaginary axis to values of S with Im $(S_n) < 0.9$ with an error of less than one percent.

To test the analytic continuation procedure for noisy data, a complex random error term was added to $f(S)$ prior to continuation. The values of $f(S)$ with the added error are

$$f_e(S_i) = f(S_i)(1 + A_R R_i)$$

$$S_i = j\omega_i l/c, \qquad i = 0,\ 1,\ 2,\ \cdots,\ 180, \tag{17}$$

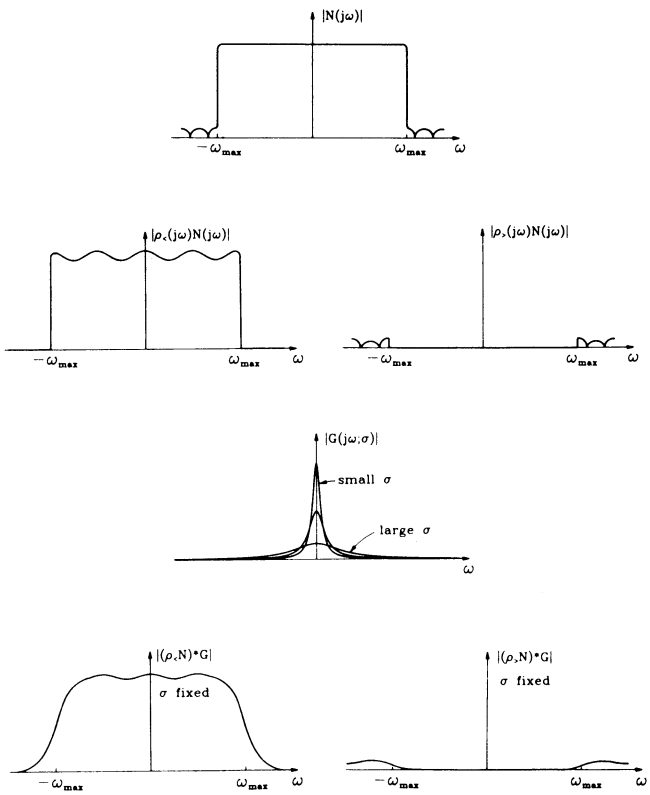

Fig. 2. Graphical representation for the functions that make up $\rho(\sigma + j\omega)$.

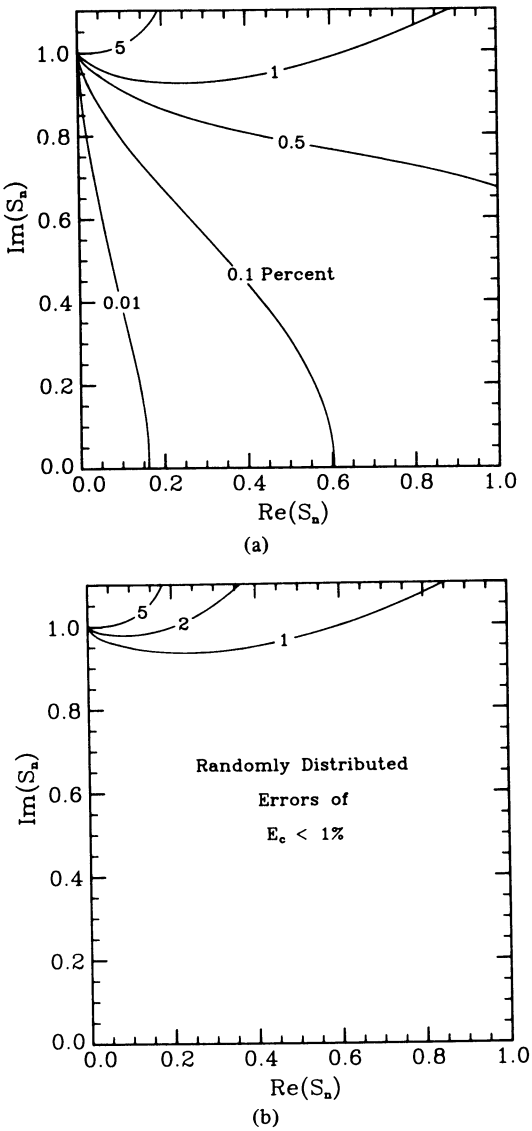

Fig. 3. Contour graphs of the error E_c (percent) in the analytic continuation procedure using the 40 dB elliptic filter. (a) For no error in the values of the normalized admittance that are analytically continued, $A_R = 0$. (b) For a 1 percent error in the values of the normalized admittance that are analytically continued, $A_R = 0.01$.

where $f(S_i)$ is the true value obtained from (5), A_R is the amplitude of the random error term, and R_i is a complex random variable that has a magnitude uniformly distributed between 0 and 1 and has a phase uniformly distributed between 0 and 2π. Fig. 3(b) shows the error (16) in the analytic continuation of $f(S)$ when the amplitude of the random error added to the admittance is one percent ($A_R = 0.01$). A comparison of Figs. 3(a) and 3(b) shows that the addition of the random error has little effect on the error in the continuation when Im $(S_n) \gtrsim 0.9$, $E_c \gtrsim 1.0$ percent (the upper portion of the graphs). These errors, $E_c \gtrsim 1.0$ percent, are mainly due to the limitations imposed on the continuation procedure by the omission of the second term on the right side of (14). Over the remainder of the graph in Fig. 3(b), the error is less than one percent, $E_c < 1.0$ percent, and randomly distributed.

Other considerations involved in the selection of the causal window function $N(s)$ used in the analytic continuation are discussed [4].

IV. The Inverse Function

The function $f(S)$ for the open-circuited coaxial line or for the monopole antenna is single valued, but the inverse function $f^{-1}(W)$ is multivalued. The problems than can arise due to this multivaluedness must be understood when $f^{-1}(W)$ is used to determine S and $\tilde{\epsilon}_r$ in the measurement procedure, (3) and (4).

The inverse function for the open-circuited coaxial line was recently studied in detail [3], and two problems were identified that are also relevant to the inverse function for the monopole antenna. First, there is a possibility that the inverse can pass onto the wrong branch, particularly when there are errors in the measurement. In this event, the wrong value of $S = f^{-1}(W)$ is selected for a particular measured value of W. An inversion procedure was developed that can keep the inverse on the correct branch, and the effectiveness of this procedure was demonstrated with measured data for the coaxial line. This procedure can also be used with the monopole antenna.

The second problem is more subtle. Even if the inversion is on the correct branch, an error in the measured W can cause an error in S and in $\tilde{\epsilon}_r$. The inversion process can make the relative error in S either larger or smaller than the relative error in W. The former is true when the measured W places S near one of the points S_{bi}. The reason for the increased error near these points is fairly simple. At these points

$$f'(S)|_{S_{bi}} = 0, \tag{18}$$

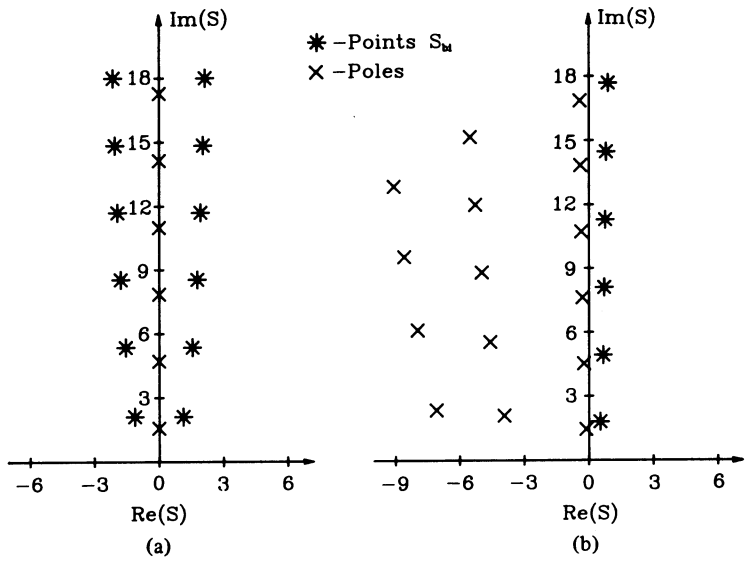

Fig. 4. Points S_{bi} and the poles. (a) Open-circuited coaxial line. (b) Cylindrical antenna. Note that $S = sl/c$ for the coaxial line, and $S = sh/c$ for the antenna.

thus at or near these points a small error in W can produce a large error in S. The points S_{bi} correspond to branch points W_{bi} of $f^{-1}(W)$ in the W plane.

For the open-circuited coaxial line, the points S_{bi} are easily determined by applying (18) to the analytical formula for $f(S)$ (5), and the locations of these points in the S plane are shown in Fig. 4(a). For the monopole antenna, there is no simple analytical formula for $f(S)$ that can be used to determine these points; however, the following procedure can be used with the measured reflection coefficient for the antenna to numerically determine $f'(S)$ and the points S_{bi}. After differentiation (2a) becomes

$$f'(S) = [Y(s) + sY'(s)]/Y_0, \tag{19}$$

and when $\rho(s)$ is introduced

$$f'(S) = \frac{1 - \rho^2(s) - 2s\rho'(s)}{[1 + \rho(s)]^2}. \tag{20}$$

Now $\rho'(s)$ is obtained from $\rho'(j\omega)$ by the formula for analytic continuation (15):

$$\rho'(s) = \frac{[\rho'_<(j\omega)N(j\omega)]^* G(j\omega;\ \sigma)}{2\pi N(\sigma + j\omega)}, \tag{21}$$

and $\rho'_<(j\omega)$ is obtained by analytically differentiating the cubic spline that is fit to the measured values of $\rho_<(j\omega)$. The points S_{bi} in the right half of the S plane for a cylindrical monopole antenna are shown in Fig. 4(b). These points were determined using the procedure described above with measured data for a monopole antenna with $h/a = 34.2$, $h_i/a = 1.33$, and $b/a = 2.30$.

The poles of $f(S)$ for the coaxial line and the monopole antenna are also shown in Fig. 4. The poles for the monopole antenna are theoretical and are for a slightly thinner antenna than the one measured [5], [6]. Note that there is more than one layer of poles for the antenna, whereas there is a single layer of poles for the coaxial line. Each of the layers for both the antenna and the coaxial line contain an infinite number of poles. The coaxial line has an infinite number of the points S_{bi} arranged in two layers that are symmetrically located about the Im (S) axis. The antenna is also expected to have an infinite number of points S_{bi} arranged in layers. There are most likely two layers of the points S_{bi} for each layer of poles. Only the points S_{bi} in the right half-plane are shown in Fig. 4(b); these are the ones of concern when using an antenna for dielectric measurements.

In Fig. 4, the points S_{bi} for the monopole antenna are seen to move to the left and down with respect to those for the coaxial line; this is what one would expect, since the poles move in a similar way.

V. Application of the Measurement Procedure

In the preceding sections, a procedure for measuring the permittivity of a material using a monopole antenna was presented, and two key elements in the procedure were described: the analytic continuation of the function $f(S)$ and the formation of the inverse $f^{-1}(W)$. Now the validity of the procedure will be established by presenting the result of measurements for materials with known dielectric properties.

A. Open-Circuited Coaxial Line

It is instructive to first consider the measurement procedure applied to the open-circuited coaxial line, Fig. 1(b). An open-circuited coaxial line was constructed from a section of APC-7 precision coaxial line. The center conductor of effective length $l = 5.20$ cm was supported by a Teflon bead of length $l_b = 2.03$ mm. The input admittance was measured with the coaxial line filled with air over the frequency range 50 MHz $\leqslant f \leqslant$ 18 GHz using a Hewlett Packard model 8409c automated network analyzer.

The coaxial line was then used to measure the permittivity

of the primary alcohol ethanol over the frequency range 50 MHz $\leqslant f \leqslant$ 8 GHz. The ethanol exhibits a Debye relaxation for the complex permittivity in this frequency range:

$$\tilde{\epsilon}_r = \epsilon_r' - j\epsilon_r'' = \epsilon_{r\infty} + (\epsilon_{rs} - \epsilon_{r\infty})/(1 + j\omega\tau). \qquad (22)$$

The three parameters in this expression ϵ_{rs}, $\epsilon_{r\infty}$, and τ have been measured at various temperatures by many investigators [7]–[12]. In Fig. 5, the measured permittivities of ethanol are plotted as a function of frequency for two cases (a) the analytic relationship (5) for $f(S)$ is used in the inversion and (b) the relationship for $f(S)$ formed from the data measured for the air-filled line with the analytic continuation procedure described in Section III is used in the inversion. The dashed lines in these graphs represent the bounds of the permittivities measured by previous investigators. These dashed lines were determined from (22) using the parameters ϵ_{rs}, $\epsilon_{r\infty}$, and τ and the variations of these parameters $\Delta\epsilon_{rs}$, $\Delta\epsilon_{r\infty}$, and $\Delta\tau$. The measured permittivities for the two cases are seen to be in good agreement with each other and also be in good agreement with the results of previous investigators. This validates the analytic continuation procedure.

The points S_{bi} for the coaxial line were also computed in two ways—from the analytic relationship (5) with (18) and from the formula based on the analytic continuation procedure (20) with (18). In Table I, the points computed by the two methods are seen to be in good agreement.

Note, in Fig. 5 the deviations in the measured permittivities are larger for both cases near the frequency 1.3 GHz. The path of the normalized propagation constant S is shown in Fig. 6. The asterisks indicate the points S_{bi}; recall that the regions of high error surround these points. The path of the normalized propagation constant is seen to pass close to one of these points. This is the cause of the increased deviation in the measured permittivities near 1.3 GHz in Fig. 5.

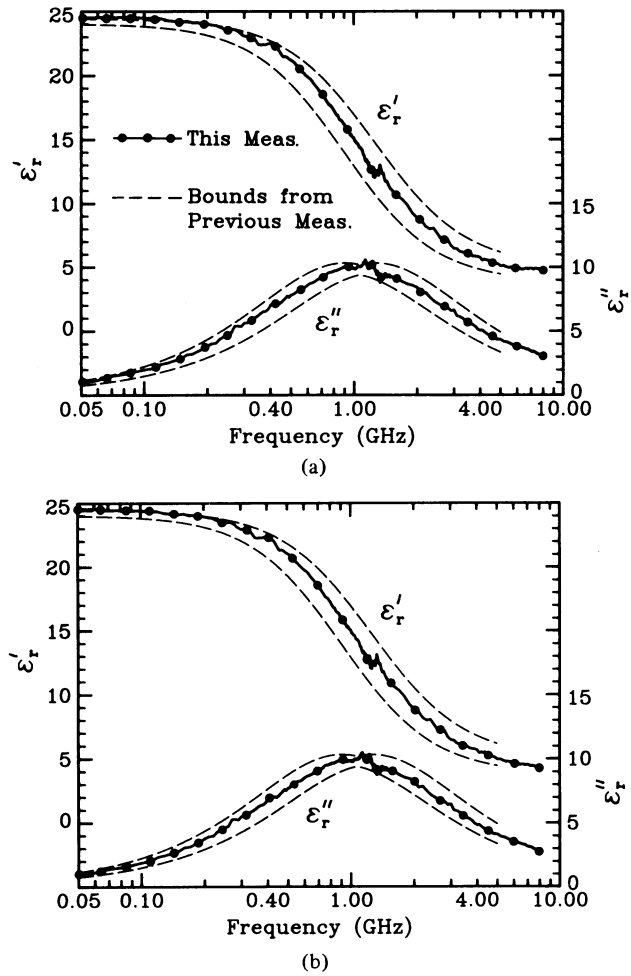

Fig. 5. Complex permittivity as a function of frequency for ethanol measured with the open-circuited coaxial line, $T = 26°C$, $l = 5.2$ cm. (a) The analytic relationship for $f(S)$ is used in the inversion. (b) The relationship for $f(S)$ formed with the analytic continuation procedure is used in the inversion.

B. Cylindrical Monopole Antenna

Measurements were also made with several different monopole antennas. The results that are presented here are for a cylindrical monopole of length $h = 5.20$ cm and radius $a = 1.52$ mm. The Teflon bead supporting the antenna had a length $l_b = 1.95$ mm and was recessed into the APC-7 coaxial line to the depth $h_i = 2.02$ mm. The input admittance of this antenna was measured in air over the frequency range 50 MHz $\leqslant f \leqslant$ 18 GHz. For these measurements, the antenna was mounted at the center of an aluminum image plane (117 cm by 152 cm) surrounded by absorbing material to reduce unwanted reflections. Fig. 7 is a graph of the measured input admittance versus frequency. Note that the effective length of the antenna is more than three wavelengths at 18 GHz ($S = j19.6$). The function $f(S)$ was formed from the measured input admittance of the antenna in air with the analytic continuation procedure described in Section III. When the input admittance is measured with the antenna immersed in a material, the complex permittivity $\tilde{\epsilon}_r$ of the material can be determined for all values of $S = j\omega\sqrt{\tilde{\epsilon}_r}h/c$ such that Im $(S) \lesssim 19.6$. That is, the values of S must be within the range in Fig. 3 where the analytic continuation is valid. Note, for a measurement technique like that described in [1] that is applicable for antennas less than or equal to resonant size, the restriction on Im (S) is much more severe, Im $(S) \lesssim 1.5$. For the procedure described in this paper, the range of applicable Im (S) can be extended by simply measuring the input admittance of the antenna in air over a larger frequency range.

Fig. 8 is an alternate representation for the admittance of the cylindrical antenna in air. This is a graph of the imaginary part of the normalized admittance W versus the real part. The curve is seen to form a succession of closed loops, with each loop surrounding one of the branch points W_{bi}. From the form of this graph, it can be argued that each of these branch points is of first order [4].

The cylindrical antenna was used to measure the permittivity of the primary alcohol, 1-butanol. This alcohol exhibits a Debye relaxation for the complex permittivity as described by (22). For this measurement, the antenna was placed in a hemispherical plastic tank of radius 21 cm attached to a metal image plane; Fig. 9 is a drawing of the tank. The tank was filled with the alcohol, the input admittance of the antenna was measured, and the permittivity was obtained by inverting the measured input admittance. The measured permittivities of the 1-butanol are shown in the Argand diagram in Fig. 10 and are

TABLE I
COMPARISON BETWEEN THE EXPERIMENTALLY AND ANALYTICALLY DETERMINED POINTS S_{bi}; BRANCH POINTS W_{bi} ARE ALSO COMPARED

	Analytic		Experimental	
i	S_{bi}	W_{bi}	S_{bi}	W_{bi}
0	0	0	0	0
1	1.13 +j 2.11	1.65 +j 2.06	1.12 +j 2.10	1.64 +j 2.06
2	1.55 +j 5.36	2.06 +j 5.33	1.54 +j 5.35	2.04 +j 5.34
3	1.78 +j 8.54	2.28 +j 8.52	1.77 +j 8.51	2.25 +j 8.55
4	1.93 +j 11.70	2.43 +j 11.69	1.91 +j 11.64	2.34 +j 11.80
5	2.05 +j 14.85	2.55 +j 14.85	2.01 +j 14.80	2.37 +j 15.07
6	2.14 +j 18.00	2.64 +j 18.00	1.91 +j 18.37	1.94 +j 17.81

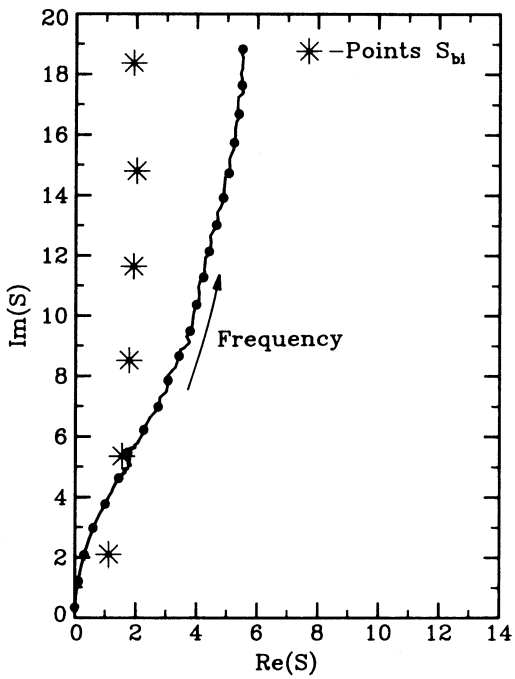

Fig. 6. Graph of the normalized propagation constant for ethanol measured with the open-circuited coaxial line, $T = 26°C$, $l = 5.2$ cm.

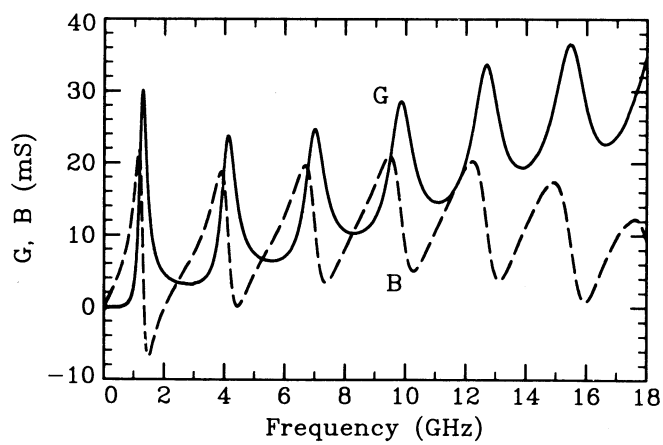

Fig. 7. Measured input admittance as a function of frequency for the cylindrical antenna in air.

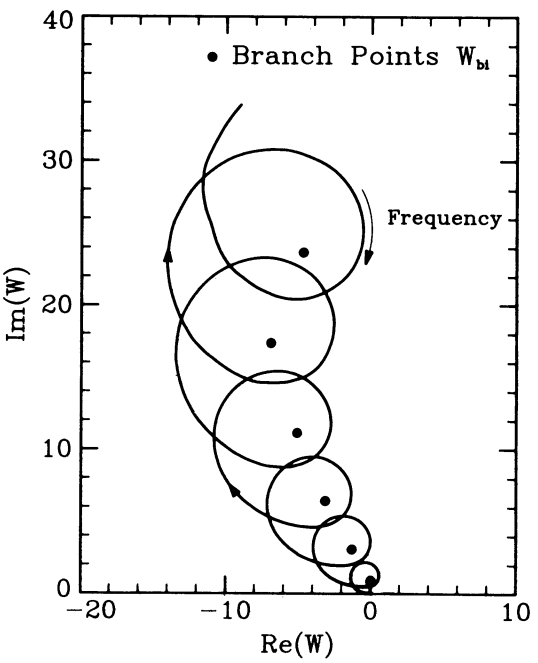

Fig. 8. Imaginary part of the normalized admittance versus the real part of the normalized admittance for the cylindrical antenna in air.

graphed as functions of frequency in Fig. 11. The permittivities are seen to be in good agreement with the values measured by previous investigators [7]–[15], except for a few of the measured points near approximately 200 MHz and near 600 MHz. The small deviation near 200 MHz is due to reflections from the side of the tank. Fig. 12 is a graph of the normalized propagation constant S. The path of S passes close to one of the points S_{bi}; this is the cause of the deviation near 600 MHz. At the highest frequencies (f near 10 GHz), the measured values of S deviate from the solid curve; this is due to the dispersion in $\tilde{\epsilon}_r$ in addition to the Debye relaxation, indicating the possible onset of a second relaxation.

The cylindrical antenna was also used to measure the permittivity of two aqueous NaCl solutions. For this measurement, the antenna was mounted on an aluminum image plane that is attached to the side of a large rectangular tank filled

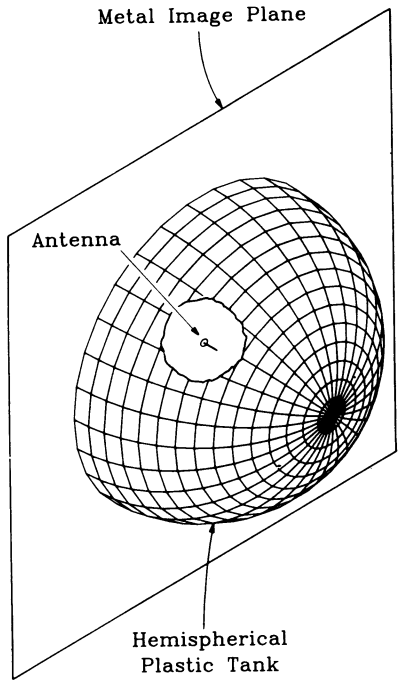

Fig. 9. Hemispherical tank mounted on an image plane, radius = 21 cm.

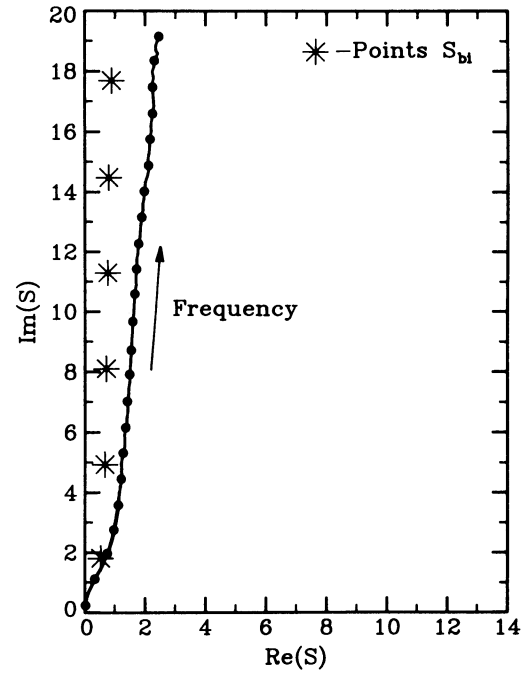

Fig. 12. Graph of the normalized propagation constant for 1-butanol measured with the cylindrical antenna, T = 23°C.

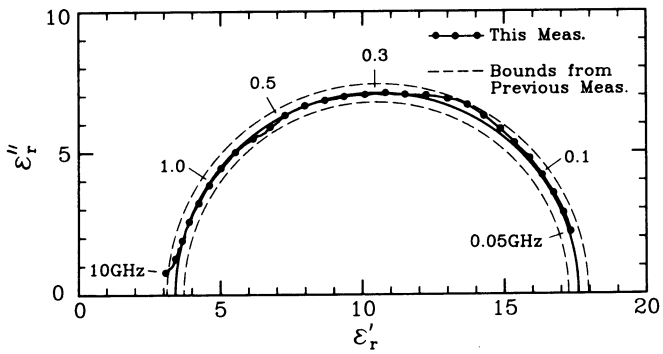

Fig. 10. Argand diagram of the complex permittivity for 1-butanol measured with the cylindrical antenna, T = 23°C.

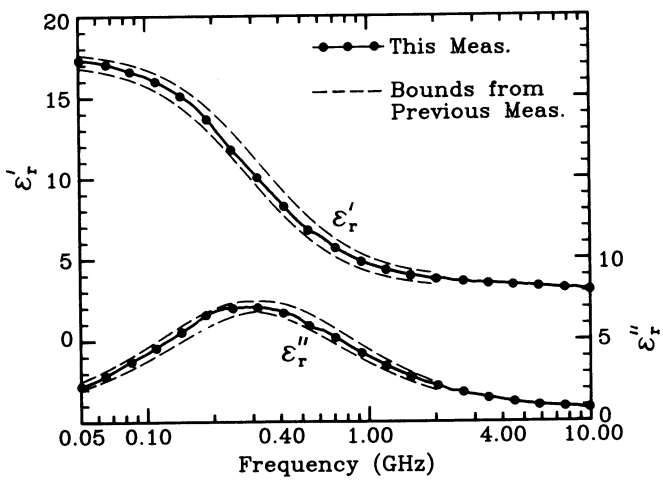

Fig. 11. Complex permittivity as a function of frequency for 1-butanol measured with the cylindrical antenna, T = 23°C.

with the solution; Fig. 13 is a drawing of the tank. The complex effective permittivities of the saline solutions are accurately described by a Debye relaxation (22) plus a term to account for the ionic conductivity:

$$\tilde{\epsilon}_r = \tilde{\epsilon}'_r - j\tilde{\epsilon}''_r = \epsilon_{r\infty} + (\epsilon_{rs} - \epsilon_{r\infty})/(1 + j\omega\tau) - j\sigma'/\omega\epsilon_0. \quad (23)$$

The two parameters ϵ_{rs} and τ are functions of the temperature and the normality of the solution; expressions for these parameters, determined from measured data, are available [16]. The third parameter $\epsilon_{r\infty}$ is approximately independent of the temperature and the normality of the solution. The ionic conductivity was measured with a conductance cell at a frequency of 20 kHz. The effective permittivity $\epsilon_{er} = \tilde{\epsilon}'_r$ and the effective conductivity $\sigma_e = \omega\epsilon_0\tilde{\epsilon}''_r$ for the two saline solutions are graphed as functions of frequency in Fig. 14. The measured constitutive parameters for the two solutions, σ' = 0.10 S/m and σ' = 1.0 S/m, are seen to be in generally good agreement with the constitutive parameters determined from (22).

Fig. 15 is a graph of the normalized propagation constants for the two solutions. The path of S for the solution with σ' = 0.10 S/m passes close to two of the points S_{bi}; this is the cause of the increased error in σ_e at the higher frequencies in Fig. 14(a). The path of S for the solution with σ' = 1.0 S/m does not pass close to any of the points S_{bi}; thus, the measured constitutive parameters do not have a region of high error.

The measured constitutive parameters of the saline solution with σ' = 1.0 S/m are seen to be noisy. A simple explanation for the cause of the noisy data is presented next. The reflection coefficient $\rho(j\omega)$ of the antenna is measured, and the admittance is determined from the reflection coefficient by (6). An expression relating the error in the admittance ΔY to a small error in the reflection coefficient $\Delta\rho$ is obtained by

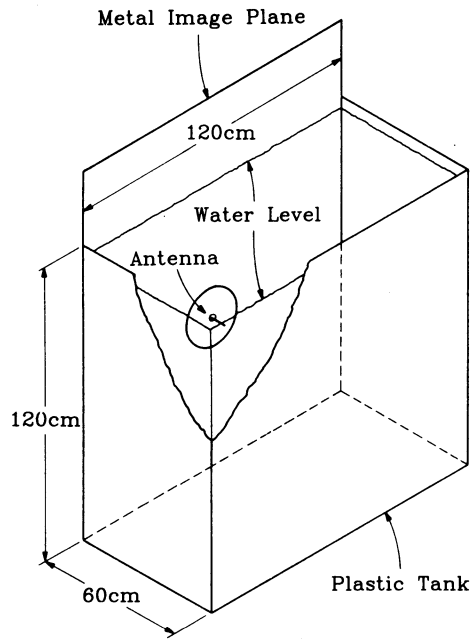

Fig. 13. Large rectangular tank with image plane.

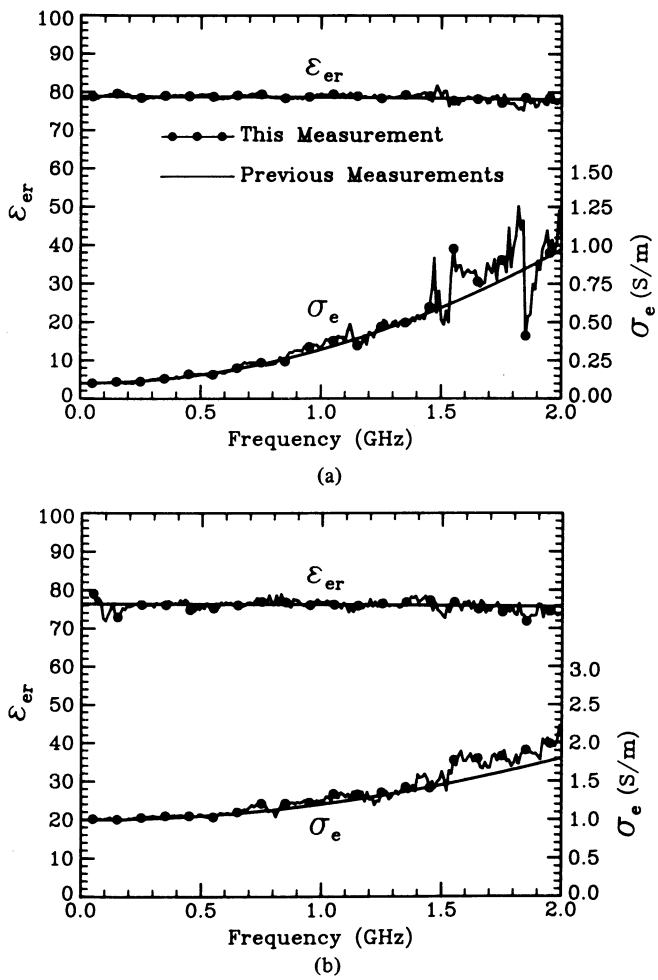

Fig. 14. Effective permittivity and effective conductivity for saline solutions measured with the cylindrical antenna. (a) $\sigma' = 0.10$ S/m, $T = 23°C$. (b) $\sigma' = 1.0$ S/m, $T = 25°C$.

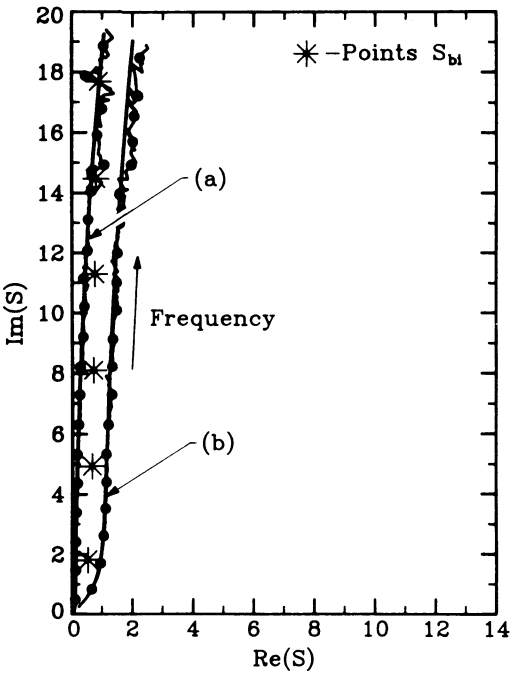

Fig. 15. Graph of the normalized propagation constants for saline solutions measured with the cylindrical antenna. (a) $\sigma' = 0.10$ S/m, $T = 23°C$. (b) $\sigma = 1.0$ S/m, $T = 25°C$.

considering a Taylor series expansion of (6):

$$|\Delta Y/Y| \approx M|\Delta\rho/\rho|, \tag{24}$$

where the multiplier M for the relative error is

$$M = |2/(1-\rho^2)|. \tag{25}$$

The multiplier is large when $\rho \approx 1$ or -1. The reflection coefficient for the antenna in the saline solutions with $\sigma' = 1.0$ S/m is close to -1, particularly at the higher frequencies. Thus, M is large (at 2.0 GHz, $|\rho| \approx 0.85$, and $M \approx 7.2$). Small errors in the measured reflection coefficient, therefore, become larger errors in the admittance and in the constitutive parameters determined from the admittance.

The measurement procedure is not limited to cylindrical monopole antennas. Measurements were also made with a conical monopole of half-angle 30°, and the accuracy for the measured constitutive parameters was comparable to that obtained with the cylindrical monopole [4].

VI. Reflections from Material Boundaries

The monopole antenna is an open structure that radiates into the surrounding medium. When the medium is finite in extent, the radiation is reflected from the boundaries of the medium, and it may cause the measured admittance for the antenna to deviate from that for an antenna in an infinite medium. At very low frequencies where the monopole is electrically short, the radiation from the antenna is very small. Thus, the amplitude of the reflections is very small, and they have little effect on the admittance. At very high frequencies where materials are fairly dissipative, the radiation and the reflections are absorbed in the material surrounding antenna. Again, the amplitude of the reflections is small, and they have little effect

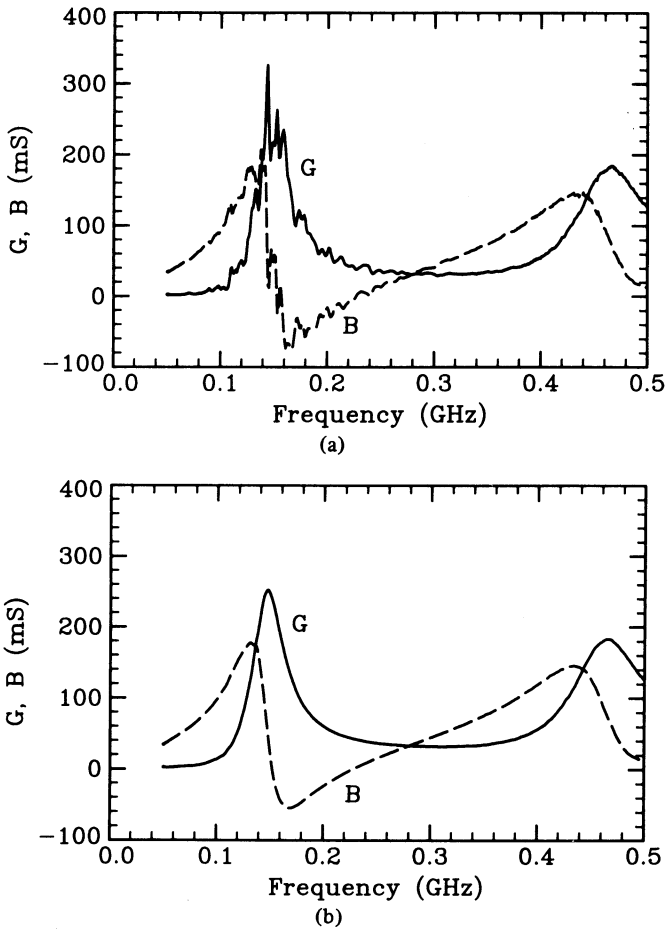

Fig. 16. Admittance of the cylindrical antenna in fresh water, $\sigma' = 8.0 \times 10^{-3}$ S/m, $T = 22°C$. (a) Uncorrected, note the ripples due to the reflections from the walls of the tank. (b) Corrected.

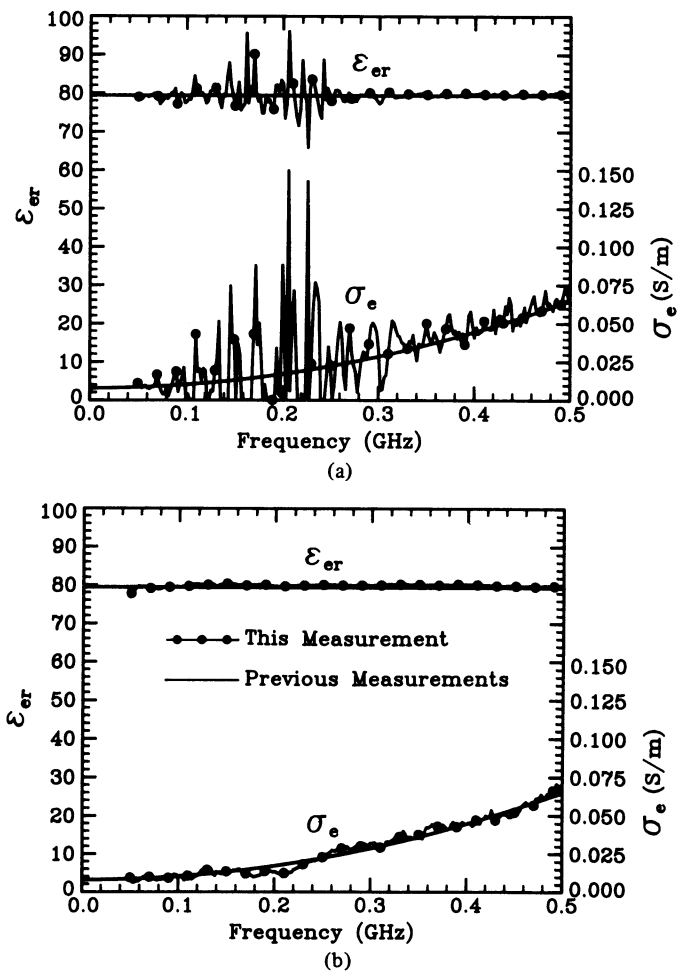

Fig. 17. Effective permittivity and effective conductivity of fresh water measured with the cylindrical antenna, $\sigma' = 8.0 \times 10^{-3}$ S/m, $T = 22°C$. (a) Obtained from the uncorrected admittance. (b) Obtained from the corrected admittance.

on the admittance. It is at the frequencies intermediate to these two extremes where the reflections have the largest effect on the input admittance of the antenna and on the determination of the constitutive parameters of the surrounding medium. This point is clearly demonstrated by the results in Figs. 10 and 11, where the finite size of the tank is seen to affect the measured permittivity only at frequencies in the range 150 MHz $\lesssim f \lesssim$ 250 MHz. In certain instances, signal processing can be used to remove the effects of the reflections from the material boundaries, as demonstrated by the example presented below.

The cylindrical antenna was used to measure the permittivity of fresh water with the tank shown in Fig. 13. Fig. 16(a) is a graph of the measured input admittance of the antenna in fresh water. The admittance is seen to oscillate rapidly; this is due to the reflections from the sides of the tank. Fig. 17(a) is a graph of the constitutive parameters ϵ_{er} and σ_e obtained from the measured admittance; as expected, these parameters also exhibit rapid oscillations. The frequency-domain data were transformed into the time domain to examine the reflections from the walls of the tank. Fig. 18 is the pulse reflected from the terminals of the antenna when the incident pulse is exp $\{[(t - 2.0 \times 10^{-8})/2.26 \times 10^{-9}]^2\}$. The ripples that occur for $t > 50$ ns are the reflections and the multiple reflections from the sides of the tank. These reflections can be removed by windowing them out in the time domain. The windowed pulse

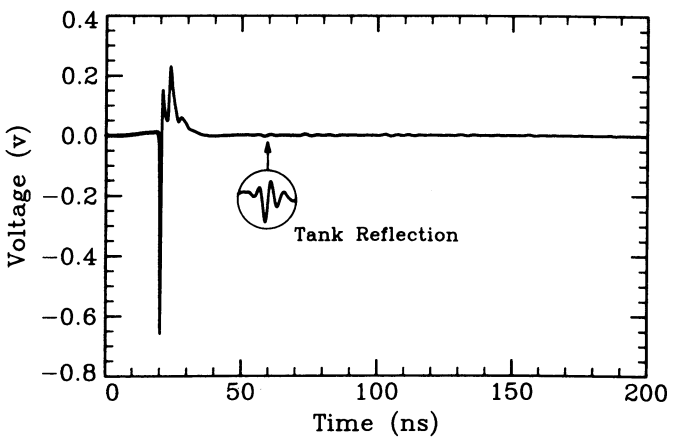

Fig. 18. Pulse reflected from the terminals of the cylindrical antenna in fresh water, $\sigma' = 8.0 \times 10^{-3}$ S/m, $T = 22°C$.

can then be transformed into the frequency domain and used to determine a corrected admittance. Fig. 16(b) is a graph of the corrected admittance; it is seen to be much smoother than the measured admittance in Fig. 16(a). Fig. 17(b) is a graph of the parameters ϵ_{er} and σ_e obtained from the corrected admittance; these parameters are much smoother and more accurate than

the parameters in Fig. 17(a) obtained directly from the measured admittance.

VII. Conclusion

A procedure was developed for using a monopole antenna to measure the complex permittivity of a material over a broad range of frequencies. The electrical size of the antenna is not restricted as in previous approaches; e.g., restricted to be electrically small or resonant. In this method, the antenna is calibrated one time by measuring the input admittance of the antenna in a standard material with a known permittivity $\tilde{\epsilon}_{rs}$, such as air, over a broad range of frequencies, $0 \leqslant \omega \leqslant \omega_{\max}$. The analytic continuation used with the calibration data is valid when Im $(S) \lesssim$ Im $(j\omega_{\max}\sqrt{\tilde{\epsilon}_{rs}}h/c)$. For example, when the calibration is in air $\tilde{\epsilon}_{rs} = 1$, the antenna can be used to measure the complex permittivity $\tilde{\epsilon}_r$ of a material at all frequencies ω such that Re $(\omega\sqrt{\tilde{\epsilon}_r}) \lesssim \omega_{\max}$.

Errors in the measurement are enhanced whenever the combination of frequency, antenna length, and material properties places the normalized propagation constant S near one of the points S_{bi}. These are the points in the S plane that correspond to the branch points W_{bi} of the normalized admittance. A similar problem was identified in a study of the open-circuited coaxial line [3]. This error can be reduced by selecting a length for the antenna so that S does not pass close to any of these points. This choice can be based on an estimate of the permittivity; however, if an estimate for the permittivity is not available, the permittivity can be measured with an antenna of convenient length, and then this permittivity can be used to obtain a better length.

The measurement procedure was verified with a series of experiments. Cylindrical and conical monopole antennas were used to measure the complex permittivity of the alcohol 1-butanol and saline solutions. Only the results for the cylindrical monopole are described in this paper. The antennas were more than three wavelengths long in the materials at the highest frequencies used in the measurements. The permittivities measured with these antennas are in good agreement with the results of previous investigators.

The greatest accuracy for this measurement procedure is obtained when the material to be measured completely surrounds the antenna and fills the recess in the coaxial line; this is no problem when measuring liquids or fine particulate matter, such as soil. For a solid material, such as rock, it would be difficult to fit the material around the antenna and the coaxial recess without producing air gaps. The errors produced by air gaps are expected to be similar to those encountered with standard coaxial line techniques when the sample being measured does not make complete contact with the inner and outer conductors.

Acknowledgment

Dr. Scott was the recipient of a TRW Foundation Augmentation Fellowship during the term of this research.

References

[1] G. S. Smith and J. D. Nordgard, "Measurement of the electrical constitutive parameters of materials using antennas," *IEEE Trans. Antennas Propagat.*, vol. AP-33, pp. 783-792, July 1985.

[2] G. A. Deschamps, "Impedance of an antenna in a conducting medium," *IEEE Trans. Antennas Propagat.*, vol. AP-10, pp. 648-650, Sept. 1962.

[3] W. R. Scott, Jr. and G. S. Smith, "Error analysis for dielectric spectroscopy using shielded open-circuited coaxial lines of general length," *IEEE Trans. Instrum. Meas.*, vol. IM-35, pp. 130-137, June 1986.

[4] W. R. Scott, Jr., "Dielectric spectroscopy using open-circuited coaxial lines and monopole antennas of general length," Ph.D. dissertation, School of Elec. Eng., Georgia Inst. Technol., Atlanta, GA, 1985.

[5] B. K. Singaraju, D. V. Giri, and C. E. Baum, "Further developments in the application of contour integration to the evaluation of the zeros of analytic functions and relevant computer programs," Air Force Weapons Lab. Math. Notes, note 42, Mar. 1976,

[6] F. M. Teshe, "Application of the singularity expansion method to the analysis of impedance loaded linear antennas," Air Force Weapons Lab. Sensor and Simulation Note, Note 177, May 1973.

[7] J. Peyrelasse, C. Boned, and J. P. LePetit, "Setting up of a time domain spectroscopy experiment, Application to the study of the dielectric relaxation of pentanol isomers," *J. Phys. E: Sci. Instrum.*, vol. 14, pp. 1002-1008, 1981.

[8] A. A. Maryott and E. R. Smith, "Table of dielectric constants of pure liquids," Nat. Bur. Stand. Circular 514, Aug. 1951.

[9] H. Nakamura, S. Mashimo, and A. Wada, "Precise and easy method of TDR to obtain dielectric relaxation spectra in GHz region," *Japanese J. Appl. Phys.*, vol. 21, no. 7, pp. 1022-1024, July 1982.

[10] F. Buckley and A. A. Maryott, "Tables of dielectric dispersion data for pure liquids and dilute solutions," Nat. Bur. Stand. Circular 589, Nov. 1958.

[11] M. W. Sagal, "Dielectric relaxation in liquid alcohols and diols," *J. Chem. Phys.*, vol. 36, no. 9, pp. 2437-2442, May 1962.

[12] A. Suggett, "Time domain methods: Dielectric and related molecular processes," *Chem. Soc. London,* vol. 1, pp. 101-120, 1972.

[13] W. Dannhauser and R. H. Cole, "Dielectric properties of liquid butyl alcohols," *J. Phys. Chem.* vol. 23, no. 10, pp. 1762-1766, Oct. 1955.

[14] A. M. Bottreau, Y. Dutuit, and J. Moreau, "On a multiple reflection time domain method in dielectric spectroscopy: Application to the study of some normal primary alcohols," *J. Chem. Phys.*, vol. 66, no. 8, pp. 3331-3336, Apr. 1977.

[15] R. Chahine and T. K. Bose, "Comparative studies of various methods in time domain spectroscopy," *J. Phys. Chem.*, vol. 72, no. 2, pp. 808-815, Jan. 1980.

[16] A. Stogryn, "Equations for calculating the dielectric constant of saline water," *IEEE Trans. Microwave Theory Tech.*, vol. MIT-19, pp. 733-736, Aug. 1971.

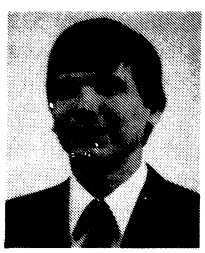

Waymond R. Scott, Jr. (S'81-M'85) was born in Calhoun, GA, on April 6, 1958. He received the B.E.E., M.S.E.E., and Ph.D. degrees from the Georgia Institute of Technology, Atlanta, in 1980, and 1985, respectively.

From 1979 to 1980, he was a Student Assistant and Graduate Research Assistant at the Georgia Tech Research Institute. From 1980 to 1985, he was a Graduate Research Assistant in the School of Electrical Engineering at the Georgia Institute of Technology, where he is currently an Assistant Professor of Electrical Engineering.

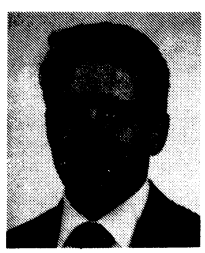

Glenn S. Smith (S'65-M'72-SM'80-F'86) was born in Salem, MA, on June 1, 1945. He received the B.S.E.E. degree from Tufts University, Medford, MA, in 1967 and the S.M. and Ph.D. degrees in applied physics from Harvard University, Cambridge, MA, in 1968 and 1972, respectively.

From 1972 to 1975 he served as a Postdoctoral Research Fellow at Harvard University and also as a part-time Research Associate and Instructor at Northeastern University, Boston, MA. In 1975, he joined the faculty of the Georgia Institute of Technology, Atlanta, GA, where he is currently Professor of Electrical Engineering.

Dr. Smith is co-author of the book, *Antennas in Matter: Fundamentals, Theory and Applications.*